| PAPER |

Simultaneous Decoupling and Matching Technique for Short-Range MIMO

Kentaro MURATA[†a)], Naoki HONMA[††], *Members*, Kentaro NISHIMORI[†††], *Senior Member*, Naobumi MICHISHITA[†], *Member*, and Hisashi MORISHITA[†], *Fellow*

SUMMARY This paper presents a novel simultaneous decoupling and matching technique for transmitting (Tx) and receiving (Rx) ports in short-range multiple-input multiple-output (SR-MIMO) systems. The principal difference with conventional decoupling and matching network (DMN) approaches is that the proposed technique considers strong mutual coupling between closely-positioned Tx/Rx arrays, and the S-parameter variation due to the presence of each other's array. This technique has two stages; first, 180-degree hybrid couplers are connected to both Tx/Rx ports of a plane-symmetrical MIMO system. This decouples both Tx/Rx ports, and moreover, channels between them are orthogonalized. That is, the MIMO system is transformed into multi orthogonalized single-input single-output (SISO) systems. Second, Tx/Rx ports of each orthogonalized SISO system are simultaneously matched based on conjugate matching theory. Consequently, the transmission power of the short-range MIMO system is maximized. Numerical results show that the proposed technique realizes higher channel capacity than the conventional DMN; indeed it achieves the theoretically possible capacity. In addition to theoretical analyses, we provide an example for microstrip line (MSL) circuit implementation. This MSL model offers good simultaneous decoupling and matching performance yielding channel capacity comparable to that of an ideally-designed circuit model. This validates the implementation feasibility of the proposed technique.

key words: short-range MIMO, decoupling and matching network

1. Introduction

Short-range communication is playing a key role in the realization of seamless connectivity, and data transfer between mobile and stationary devices is envisioned as one of the main applications. In order to deal with Gbit/s-order large-volume data sets such as movies and images, ultra wide band (UWB) and millimeter-wave technologies are used that can increase the transmission capacity per unit of time [1]. A different approach to enhancing frequency utilization efficiency is short-range multiple-input multiple-output (SR-MIMO) communication [2]–[4].
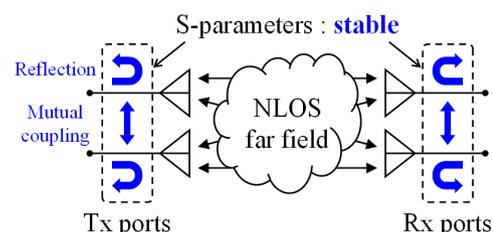
Literally, "short-range MIMO" is a MIMO technique intended for short-range communication wherein Tx/Rx arrays face to each other with line-of-sight (LOS) links. Its usage scenarios include wall-the-through repeaters [5] and

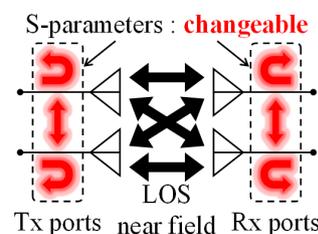peer-to-peer communication between digital KIOSK and mobile terminals [6].

In our previous work, we focused on the characteristics of SR-MIMO, its propagation channels are uniquely determined due to its LOS configuration, and proposed an analog-beamforming-based eigenmode transmission technique [7]–[9]. In this technique, by connecting 180-degree hybrid couplers (HCs) to both Tx/Rx sides of a plane-symmetrical SR-MIMO system, the MIMO channels are orthogonalized into multi independent streams using only analog passive networks which greatly reduces hardware complexity.

However, while the channel characteristics of SR-MIMO have been well analyzed, antenna characteristic problems such as reflection and mutual coupling, all of which can degrade channel capacity, have not been addressed. Solving these problems allows the maximum channel capacity of a SR-MIMO system to be realized.

A typical approach to improve the radiation efficiency and envelope correlation of a MIMO array is the use of decoupling and matching networks (DMN) [10]–[16]. These conventional DMN approaches assume that Tx/Rx arrays exist in non-LOS (NLOS) and far field configurations as shown in Fig. 1(a). In such a case, the Tx/Rx S-parameters

(a) Array S-parameters in NLOS far field.

(b) Array S-parameters in LOS near field.

Fig. 1 Assumed situations for conventional and proposed approaches.

are independent of the existence of the array on the other side. Thus, Tx/Rx DMNs can be designed independently based on only the Tx/Rx S-parameters, respectively. However, in short range communication, undoubtedly near field as shown in Fig. 1(b), the Tx/Rx S-parameters are influenced by the strong mutual coupling between proximally-positioned Tx/Rx arrays. Hence, a conventional DMN preliminarily-designed for each array does not work effectively, if anything, it may worsen performance due the matching condition on the other side. Such interaction between Tx/Rx arrays makes it difficult to satisfy decoupling and matching conditions on both sides simultaneously.

On the other hand, Roberts established the theory of conjugate-image impedances, which allows simultaneous matching at both Tx/Rx sides in the presence of mutual coupling [17] (A similar approach can be seen in [18] but with a different mathematical presentation.) For reference, Inagaki applied this theory to wireless power transfer (WPT) between inductively coupled coils to maximize transfer efficiency [19]. However, this concept is valid only for a two-port network, i.e. single-input single-output (SISO) systems, so it cannot be extended to MIMO systems directly.

In order to provide a comprehensive solution to the above problems, we proposed the bidirectional matching technique for SR-MIMO [20] by combining the aforementioned conventional ideas. This technique has two stages; first, the SR-MIMO system is orthogonalized into several SISO systems by HCs. Second, Tx/Rx ports are simultaneously matched by applying the conjugate image impedance theory to each orthogonalized SISO system individually. Finally, the whole SR-MIMO system is fully matched.

As possible target scenarios of the proposed technique, we envision its application to the SR-MIMO systems operated in wireless data transfer and video streaming involving mobile devices as shown in Fig. 2(a) and (b), respectively [21]. The proposed technique can overcome the following negative factors faced in such applications, (i) strong mutual coupling between multi-antennas closely packed in the mobile device and (ii) mismatching caused by the proximity of the Tx/Rx MIMO arrays. As a consequence, it unleashes the potential of SR-MIMO performance.

However, [20] considers only the theoretical aspect for 2×2 SR-MIMO, while extensions to more than 2×2 and
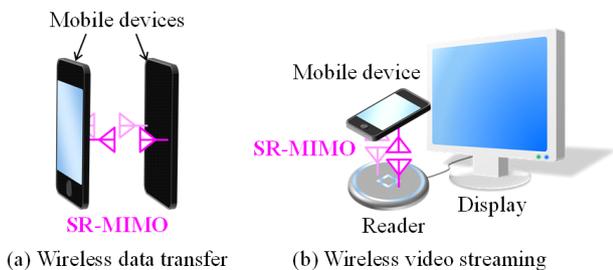
practical implementation were not mentioned.

This paper proposes an extended simultaneous decoupling and matching technique for SR-MIMO based on an S-parameter analysis; the S-parameter-based approach is efficient and simple to apply to the analysis of cascade-connected networks [22]. Furthermore, insights on an extension to, at most, 8×8 SR-MIMO is given. Finally, an example of practical circuit implementation using microstriplines (MSLs) is presented to validate the feasibility of the proposed technique.

Section 2 focuses on the theoretical aspects of the proposed technique. In Sect. 3, some numerical results are presented for a performance comparison between the proposed and conventional DMN techniques in terms of (i) simultaneous decoupling and matching effects and (ii) channel capacity improvement. Section 4 concludes the paper with application prospects and challenges posed by the proposed technique.

2. Theory of Proposed Technique

The proposed method is implemented in two steps: "port decoupling and channel orthogonalization" and "simultaneous matching". In this section, the theory of the proposed method is explained step-by-step.

2.1 Port Decoupling and Channel Orthogonalization

In order to explain the basic theory, the 2×2 SR-MIMO system shown in Fig. 3(a) is considered for simplicity. In the MIMO system, the ports from #1 to #2 and from #3 to #4

(a) Wireless data transfer   (b) Wireless video streaming

Fig. 2 Target scenarios of the proposed technique.

(a) MIMO array only.

(b) With hybrid couplers.

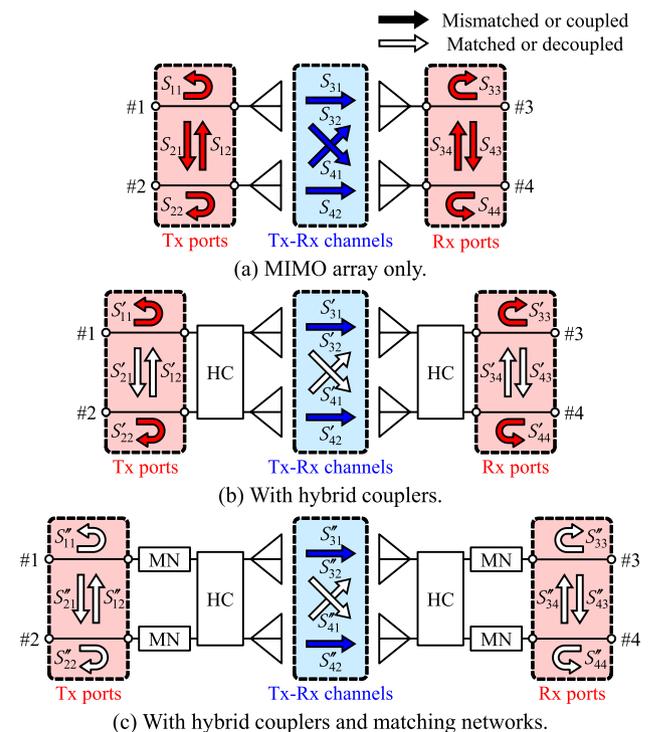(c) With hybrid couplers and matching networks.

Fig. 3 Conceptual diagram of the S-parameter on each stage.

are Tx/Rx ports, respectively. Here, we define Tx-Rx port pairs of #1 and #3, and #2 and #4, and the channel between each port pair is defined as the "signal channel", while the channel between the non-corresponding ports is defined as the "interference channel". The S-parameter of the system is defined as

$$S_{\mathrm{MIMO}} = \begin{bmatrix} S_{\mathrm{TT}} & S_{\mathrm{TR}} \\ S_{\mathrm{RT}} & S_{\mathrm{RR}} \end{bmatrix} \qquad (1)$$

$$= \begin{bmatrix} S_{11} & S_{12} & S_{13} & S_{14} \\ S_{21} & S_{22} & S_{23} & S_{24} \\ S_{31} & S_{32} & S_{33} & S_{34} \\ S_{41} & S_{42} & S_{43} & S_{44} \end{bmatrix}$$

where S_{TT} and S_{RR} represent reflections and couplings at Tx/Rx ports, respectively. S_{TR} and S_{RT}, which represent the channel matrices between Tx/Rx ports, are the transpose of each other. If the SR-MIMO array is configured symmetrically with respect to the reference plane that divides the array into two pairs of Tx/Rx antennas, submatrices S_{TT}, S_{TR}, S_{RT} and S_{RR} in (1) become symmetrical. With regard to Tx ports, reflections at ports #1, S_{11}, and #2, S_{22}, are equal and it is obvious that the couplings between them, S_{12} and S_{21}, are equal because of the reciprocity of the S-parameter. That is also true for Rx ports. Furthermore, signal channels between facing ports #1 and #3, S_{31}, and between #2 and #4, S_{42}, are equal as are the interference channels between diagonal ports #1 and #4, S_{41}, and between #2 and #3, S_{32}. Taking these matters into consideration, all submatrices in (1) can be expressed in the form of

$$\begin{bmatrix} \alpha & \beta \\ \beta & \alpha \end{bmatrix} \qquad (2)$$

where α and β are complex constants.

Next, HCs are connected to both Tx/Rx ports of the SR-MIMO system as shown in Fig. 3(b). The S-parameter of an HC, S_{HC}, is expressed as

$$S_{\mathrm{HC}} = \begin{bmatrix} S_{\mathrm{HC,ii}} & S_{\mathrm{HC,oi}} \\ S_{\mathrm{HC,io}} & S_{\mathrm{HC,oo}} \end{bmatrix} \qquad (3)$$

where index "i" and "o" denote "input" and "output", respectively. Since neither reflection nor mutual coupling occurs at either the input or output of an ideal HC,

$$S_{\mathrm{HC,ii}} = S_{\mathrm{HC,oo}} = O_2 \qquad (4)$$

where O_n denotes an nth-order zero matrix. The transmission matrices between inputs and outputs are

$$S_{\mathrm{HC,io}} = S_{\mathrm{HC,oi}} = -\frac{j}{\sqrt{2}} \begin{bmatrix} 1 & 1 \\ 1 & -1 \end{bmatrix} \qquad (5)$$

where the first and second column (or row) vectors correspond even and odd modes, respectively, and such matrix in the brackets is known as the second-order Hadamard matrix. When HCs connected to both Tx/Rx sides, the S-parameter of the whole MIMO system including HCs, S'_{MIMO}, is expressed as

$$S'_{\mathrm{MIMO}} = \begin{bmatrix} S_{\mathrm{HC,io}}S_{\mathrm{TT}}S_{\mathrm{HC,oi}} & S_{\mathrm{HC,io}}S_{\mathrm{TR}}S_{\mathrm{HC,io}} \\ S_{\mathrm{HC,oi}}S_{\mathrm{RT}}S_{\mathrm{HC,oi}} & S_{\mathrm{HC,oi}}S_{\mathrm{RR}}S_{\mathrm{HC,io}} \end{bmatrix}. \qquad (6)$$

The derivation of the above equation is explained in Appendix A in the end of the paper. As a result, all submatrices in (6) are expressed as the product of the matrices having the symmetric form of (2) and the transmission matrices of Tx/Rx HCs (given as (5)) in the form of

$$-\frac{j}{\sqrt{2}} \begin{bmatrix} 1 & 1 \\ 1 & -1 \end{bmatrix} \cdot \begin{bmatrix} \alpha & \beta \\ \beta & \alpha \end{bmatrix} \cdot -\frac{j}{\sqrt{2}} \begin{bmatrix} 1 & 1 \\ 1 & -1 \end{bmatrix} \qquad (7)$$

$$= -\begin{bmatrix} \alpha + \beta & 0 \\ 0 & \alpha - \beta \end{bmatrix}$$

and diagonalized. That means that both Tx/Rx ports are decoupled [14], and moreover, interference channels are canceled out [7]. Consequently, S'_{MIMO} has regular sparseness that is expressed as

$$S'_{\mathrm{MIMO}} = \begin{bmatrix} S'_{11} & 0 & S'_{13} & 0 \\ 0 & S'_{22} & 0 & S'_{24} \\ S'_{31} & 0 & S'_{33} & 0 \\ 0 & S'_{42} & 0 & S'_{44} \end{bmatrix} \qquad (8)$$

where diagonal components in each ruled-off submatrix are given by (8). From (8), it is found that light- and dark-colored parts form independent SISO systems between corresponding Tx-Rx port pairs. These first and second diagonal SISO systems correspond to even and odd modes of the HC, respectively. In this way, the first stage transforms the MIMO system into two orthogonalized SISO systems.

This process seemingly has a negative impact, reducing channel capacity, since some channel components are eliminated. Moreover, S'_{41} is given as the subtraction between two constants in (8). However, the Frobenius norm of the channel matrix, i.e. total transmission power, is actually constant before and after the process. This is because the transmission matrix of HC, given as (5), is unitary, and so channel capacity is never changed by the process; that is proven in Appendix B.

2.2 Simultaneous Matching

Now that the two orthogonalized SISO systems are obtained, the conventional simultaneous matching theory can be applied to each individually.

According to [23], when the reflection coefficients of Tx/Rx MNs that have their inputs or outputs terminated with reference impedances Z_0, are equal to the conjugates of the reflection coefficients looking into an arbitrary SISO system from the Tx side, Γ_{Tx}, and looking back at the Rx side, Γ_{Rx}, respectively, as shown in Fig. 4, conjugate matching conditions are simultaneously satisfied at both Tx/Rx sides. In [23], if the S-parameter of a SISO system, S_{SISO}, is defined as

$$S_{\mathrm{SISO}} = \begin{bmatrix} S_{\mathrm{TT}} & S_{\mathrm{TR}} \\ S_{\mathrm{RT}} & S_{\mathrm{RR}} \end{bmatrix}, \qquad (9)$$

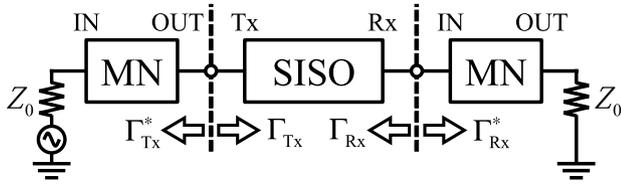equivalent reflection coefficients Γ_{Tx} and Γ_{Rx} are given as

Fig. 4 Condition of simultaneous matching for a SISO system.

$$\Gamma_{\text{Tx}} = \left(\frac{B_{\text{Tx}} \pm \sqrt{B_{\text{Tx}}^2 - 4\,|C_{\text{Tx}}|^2}}{2C_{\text{Tx}}} \right)^*$$

$$\Gamma_{\text{Rx}} = \left(\frac{B_{\text{Rx}} \pm \sqrt{B_{\text{Rx}}^2 - 4\,|C_{\text{Rx}}|^2}}{2C_{\text{Rx}}} \right)^* \qquad (10)$$

where

$$\begin{aligned} B_{\text{Tx}} &= 1 + |S_{\text{TT}}|^2 - |S_{\text{RR}}|^2 - |\Delta|^2 \\ B_{\text{Rx}} &= 1 + |S_{\text{RR}}|^2 - |S_{\text{TT}}|^2 - |\Delta|^2 \\ C_{\text{Tx}} &= S_{\text{TT}} - \Delta S_{\text{RR}}^* \\ C_{\text{Rx}} &= S_{\text{RR}} - \Delta S_{\text{TT}}^* \end{aligned} \qquad (11)$$

In the above equations, A^* and $|A|$ denote conjugate and absolute of complex number A, respectively, and Δ is the determinant of S_{SISO}. Note that, in (10), the appropriate sign must be chosen so that the absolute of each coefficient falls in the range of 0 to 1. Furthermore, [23] discusses the maximum gain, $G_{\max}$, when both Tx- and Rx-port mismatch losses are compensated; it is expressed as

$$G_{\max} = \frac{1}{1 - \left|\Gamma_{\text{Tx}}^*\right|^2} \, |S_{\text{TR}}|^2 \, \frac{1 - \left|\Gamma_{\text{Rx}}^*\right|^2}{\left|1 - S_{\text{RR}}\Gamma_{\text{Rx}}^*\right|^2}. \qquad (12)$$

Next, the design method of MN that realizes the maximum gain in (12) is detailed. Here, let the S-parameter of MN, S_{MN}, be expressed as

$$S_{\text{MN}} = \begin{bmatrix} S_{\text{MN,ii}} & S_{\text{MN,oi}} \\ S_{\text{MN,io}} & S_{\text{MN,oo}} \end{bmatrix}. \qquad (13)$$

Basically, there are two conditions that MN must satisfy. The first is the above-mentioned conjugate matching condition, and the S-parameter components $S_{\text{MN,oo}}$ and $S_{\text{MN,ii}}$ of Tx/Rx MNs are given as

$$\begin{aligned} S_{\text{MN,oo}} &= \Gamma_{\text{Tx}}^* \quad \text{for Tx MN} \\ S_{\text{MN,ii}} &= \Gamma_{\text{Rx}}^* \quad \text{for Rx MN} \end{aligned} \qquad (14)$$

The second is a unitary condition that is expressed as

$$S_{\text{MN}}^H S_{\text{MN}} = I_2 \qquad (15)$$

where A^H denotes the Hermitian transpose of matrix A and I_n is an nth-order identity matrix, and (15) indicates that the MN is lossless. By satisfying (14) and (15), the amplitudes of all components in (13) are uniquely determined, also their phases are related to each other having one degree of freedom [24].

In this way, each orthogonalized SISO system is simultaneously matched by designing the MNs individually based
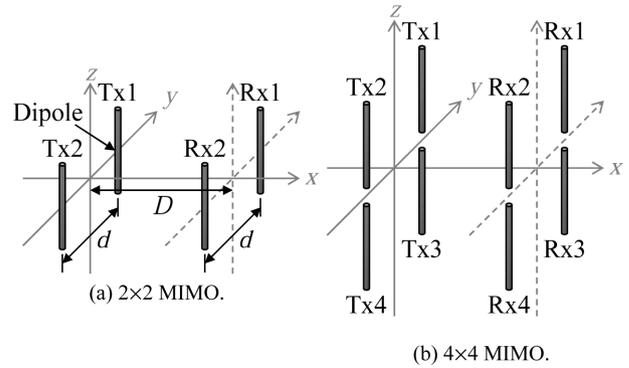

(a) 2×2 MIMO.

(b) 4×4 MIMO.

Fig. 5 Some practical configurations for application of the proposed technique.

on the above theory and then cascade-connecting them. The S-parameter of the whole MIMO system, including HCs and MNs, S_{MIMO}'', is expressed as

$$S_{\text{MIMO}}'' = \begin{bmatrix} O_2 & \begin{matrix} S_{13}'' & 0 \\ 0 & S_{24}'' \end{matrix} \\ \begin{matrix} S_{31}'' & 0 \\ 0 & S_{42}'' \end{matrix} & O_2 \end{bmatrix} \qquad (16)$$

where reflections, mutual couplings and interference channels are completely eliminated, and only signal channels exist as shown in Fig. 3(c) and are maximized as expressed in (12).

2.3 Extension to 4×4 and 8×8 SR-MIMO

In Sect. 2, we discussed the basic theory of the proposed technique for a 2×2 SR-MIMO case that is symmetrical respect to a certain plane as shown in Fig. 5(a). The above discussion indicates that, if a SR-MIMO system can be divided into multiple orthogonalized SISO systems by HCs, it is possible to apply the simultaneous matching process. In [7], it was proven that a rectangularly configured 4×4 SR-MIMO system (as shown in Fig. 5(b)) that is symmetrical with respect to vertical and horizontal reference planes can be orthogonalized using four cascade-connected HCs forming a fourth-order-Hadamard-matrix weight. Furthermore, from the geometrical perspective, it is possible to orthogonalize, at most, an 8×8 SR-MIMO system having a cuboidal configuration and three symmetry planes, in which Tx/Rx arrays are interwoven. Therefore, the proposed technique can be extended, at most, to 8×8 SR-MIMO systems.

3. Numerical Results

A 2×2 SR-MIMO system consisting of very thin half-wavelength dipoles, see Fig. 5(a), is simulated wherein Tx/Rx arrays face each other in complete LOS. Antennas Tx/Rx1-2 correspond to Tx ports #1-#2 and Rx ports #3-#4, respectively. For S-parameter calculation of the SR-MIMO array, NEC2 is used [25].

In the rest of this paper, the structural symmetry of

the system is assumed, and some S-parameters components bearing a symmetrical relationship may not be mentioned to avoid repetitive statements.

3.1 Frequency Responses

3.1.1 Simulation Condition

In this subsection, frequency characteristics are discussed. In the simulation, center frequency f_c is set to 2.5 GHz. The analysis frequency range is ±0.5% from the normalized center frequency, so the analysis bandwidth, BW, is 25 MHz. As for array parameters, antenna spacing d and Tx-Rx distance D are set to 0.1 λ and 0.25 λ, respectively. λ is the wavelength of f_c in free-space. For comparison, the S-parameter of only a single array, S, at f_c without the other is calculated as follows.

$$S = \begin{bmatrix} -6.28\angle 41.5 & -11.2\angle -82.0 \\ -11.2\angle -82.0 & -6.28\angle 41.5 \end{bmatrix} \text{dB}\angle\text{deg.} \quad (17)$$

3.1.2 Four Analysis Cases

To evaluate the simultaneous decoupling and matching effects yielded by the proposed technique, the following four cases are examined.

(i) Without DMN: The first case, defined as "w/o DMN", applies neither decoupling nor matching technique. In the above condition, the S-parameter submatrices of the SR-MIMO system at f_c are calculated as
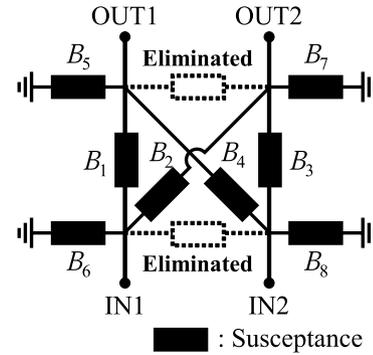
$$S_{TT} = \begin{bmatrix} -5.38\angle 72.3 & -15.9\angle -65.2 \\ -15.9\angle -65.2 & -5.38\angle 72.3 \end{bmatrix} \text{dB}\angle\text{deg} \quad (18)$$

$$S_{TR} = \begin{bmatrix} -5.50\angle -35.4 & -21.4\angle -112.1 \\ -21.4\angle -112.1 & -5.50\angle -35.4 \end{bmatrix} \text{dB}\angle\text{deg.} \quad (19)$$
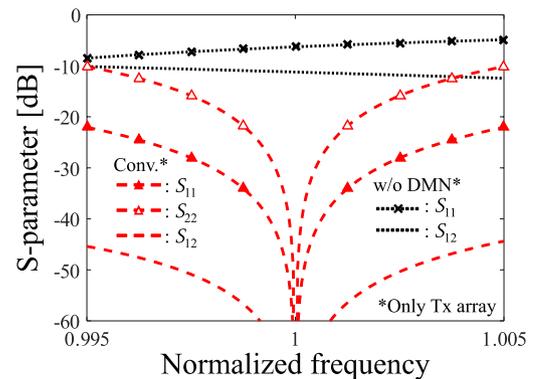
The most important point is that S_{TT} is varied from (17) due to the presence of the Rx array.

(ii) With conventional DMN: The second case, defined as "Conv.", applies conventional multiport-conjugate-match (MCM) DMN [10]–[12]; basically, the MCM-based approach can be universally applied to any MIMO antennas without specific requirements.

The DMN is designed based on the S-parameter of only a single array expressed as (17). In this paper, we use a typical DMN configuration consisting of susceptances as shown in Fig. 6(a) [13]. Although there should originally be two more susceptances between inputs and between outputs (indicated by the dotted lines), they can be eliminated by optimization; in fact, the MCM approach provides infinite degrees of freedom in terms of circuit design. The values of susceptances $B_1 \sim B_8$ are shown in Table 1; a capacitor is used if the susceptance is positive, while an inductor is used if it is negative. For port correspondence, OUT1 and OUT2 of the DMN are connected to antennas Tx1 and Tx2, respectively. Its IN1 and IN2 correspond to Tx ports #1 and

(a) Circuit configuration.

(b) S-parameter characteristics.

Fig. 6 Conventional DMN.

Table 1 Susceptances of conventional DMN in mS.

B_1	B_2	B_3	B_4	B_5	B_6	B_7	B_8
9.44	9.44	13.7	−13.7	7.16	−14.4	−20.3	−32.6

#2, respectively. Likewise, the same DMN is also connected to the Rx array. The S-parameter characteristics when the DMN is used are shown in Fig. 6(b). Note that only the Tx array is considered in the simulation. From the figure, the DMN enables perfect decoupling and matching at f_c.

(iii) With proposed DMN with ideal implementation: The third case, defined as "Ideal", employs the proposed technique implemented with ideal circuit design as shown in Fig. 7.

The transmission-line (TL) rat-race HC (Fig. 7(a)) operates ideally as expressed (4) and (5) at f_c. However, it is frequency-dependent due to the fixed TL length while its characteristic impedance is constant at $\sqrt{2}Z_0$ (Z_0 is 50 Ω). Taking the Tx side as an example, OUT1 and OUT2 of the HC are connected to antennas Tx1 and Tx2, respectively. Its IN1 and IN2 correspond to even and odd modes of the hybrid, and different MNs are individually designed for each mode.

As the simplest MN configuration, the L-section inductor-capacity (LC) MN (Fig. 7(b)) is used. The values
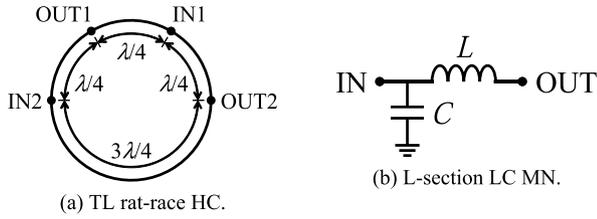
(a) TL rat-race HC.

(b) L-section LC MN.

Fig. 7 Ideal circuit model.

(a) MSL rat-race HC.

(b) Single-shunt MSL MN.

Fig. 8 Practical circuit model.

of inductor L and capacitor C of the even- and odd-mode MNs are determined to satisfy the simultaneous matching condition as explained in Sect. 2.2 and listed in Table 2(a). The inputs of the even- and odd-mode MNs correspond to Tx ports #1 and #2, respectively. While inputs and outputs of the HC are reversible due to the symmetrical circuit configuration, attention should be paid to the orientation of the MN at the Rx side; should we follow the connection rule shown in Fig. 4, IN and OUT of the MN shown in Fig. 7(b) must be switched on the Rx side.

(iv) With proposed DMN with practical implementation: The fourth case, defined as "Prac.", also employs the proposed technique but a more practical MSL circuit arrangement is used as shown in Fig. 8.

Figure 8(a) and (b) show a MSL rat-race HC and single-shunt MN, respectively. They are individually assumed to exist on an infinite dielectric substrate with thickness of 1.56 mm, permittivity of 2.2 and dielectric tangent of 0.0008. For MSL analysis, IE3D is used [26] and circuit parameters are optimized. The width and length of the rat-race ring are as shown in the figure, and design parameters of the MN are shown in Table 2(b). For comparison with the ideal HC, the S-parameter submatrices, $S'_{HC,ii}$ and $S'_{HC,io}$, of the practical one at f_c are as follows.

$$S'_{HC,ii} = \begin{bmatrix} -38.8\angle 87.9 & -57.3\angle 39.1 \\ -57.3\angle 39.1 & -44.2\angle 128.8 \end{bmatrix} \text{dB}\angle\text{deg} \quad (20)$$

$$S'_{HC,io} = \begin{bmatrix} -3.14\angle 0 & -3.12\angle 0.24 \\ -3.12\angle 0.07 & -3.13\angle 179.9 \end{bmatrix} \text{dB}\angle\text{deg} \quad (21)$$

where the phases in (21) are normalized by that of the upper-left element. The above equations indicate that reflections and mutual coupling at inputs are sufficiently reduced. Also, the transmission matrix of (5) is realized with slight loss and phase error. However, the S-parameter submatrices of the SR-MIMO system cannot be strictly diagonalized as expressed in (8) by the practical HC. In the practical model, the simultaneous matching conditions are derived without consideration of the slightly-remaining mutual coupling and interference channel components between the different-mode SISO systems.

To evaluate the design accuracy of the practical MNs, the following two parameters are defined, see also Table 3.
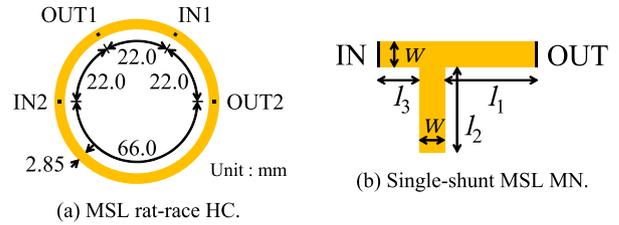
$$\rho = \frac{S'_{MN,oo}}{\Gamma^*_{Tx}} \quad (22)$$

Table 2 Design parameters of MNs.

(a) Ideal LC MN.			(b) Practical MSL MN.				
	L [nH]	C [pF]	Unit: mm	w	l_1	l_2	l_3
Even	3.06	0.924	Even	5.40	11.2	8.05	3.04
Odd	5.40	1.22	Odd	4.21	11.9	14.4	3.85

Table 3 MSL MN characteristics at center frequency.

	ρ [dB$\angle$deg]	P_{loss} [dB]
Even	$-0.02\angle 0.05$	-19.1
Odd	$0.03\angle -0.15$	-21.0

$$P_{loss} = 1 - \frac{1}{2} \left\| S'_{MN} \right\|_F^2 \quad (23)$$

where $S'_{MN,oo}$ is an element of the S-parameter matrix, S'_{MN}, of the practical MN, and $\|A\|_F$ is the Frobenius norm of matrix A. The first parameter ρ indicates how much the simultaneous matching condition of (14) is satisfied. When $\rho = 1$ (antilog), the condition is perfectly satisfied. The second parameter P_{loss} indicates losses generated by the practical MN but does not include mismatching loss. The factor $1/2$ is for normalization. $P_{loss} = 0$ (antilog) means that the unitary condition given as (15) is satisfied, i.e. the MN is lossless. From the table, both even- and odd-mode MNs can be designed with high accuracy and small loss.

Regarding the second, third and fourth cases, the S-parameter of the whole SR-MIMO system including the circuit part is rigorously computed by cascade-connecting the Tx/Rx arrays and the circuits in post-processing based on (A·2) as detailed in Appendix A.

3.1.3 S-Parameter Characteristics

Figures 9(a), (b), (c) and (d) show the frequency responses of mutual coupling, interference channel, reflection and signal channel, respectively. In the figures, the aforementioned four-case characteristics are displayed with different line types. For quantitative understanding, those at f_c are organized in Table 4.

First, mutual coupling, S_{12}, and interference channel, S_{41}, characteristics are considered. From the figures, those of the ideal model are completely suppressed at f_c as ex-
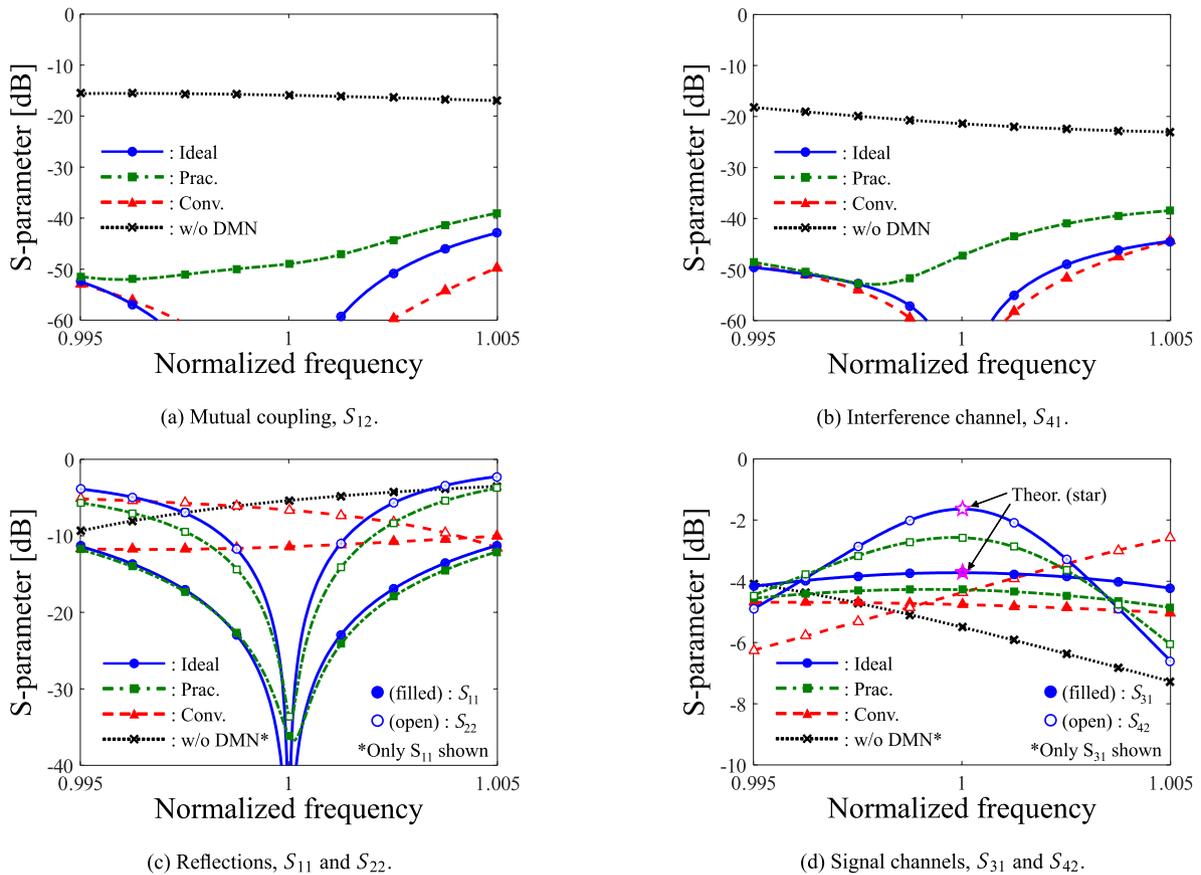
(a) Mutual coupling, S_{12}.

(b) Interference channel, S_{41}.

(c) Reflections, S_{11} and S_{22}.

(d) Signal channels, S_{31} and S_{42}.

Fig. 9 Frequency responses of S-parameter.

Table 4 S-parameter components at center frequency.

	Unit: dB	w/o DMN	Conv.	Prac.	Ideal	Theor.
Fig. 9(a)	S_{12}	−15.9	−∞	−48.9	−∞	−∞
(b)	S_{41}	−21.4	−∞	−47.2	−∞	−∞
(c)	S_{11}	−5.38	−11.4	−36.1	−∞	−∞
	S_{22}	−5.38	−6.63	−33.7	−∞	−∞
(d)	S_{31}	−5.50	−4.76	−4.28	−3.72	−3.72
	S_{42}	−5.50	−4.37	−2.57	−1.64	−1.64

pressed in (8). Although those of the practical model cannot be completely reduced due to the design error of the MSL HC, they remained below −40 dB or so over the analysis range of frequencies. Other interesting point is that conventional model also allows perfect decoupling and interference channel suppression despite the S-parameter variation due to the presence of the opposite array. This can be interpreted as follows; turning back to the conventional DMN configuration shown in Fig. 6, if a current is imposed on IN1, it is equally distributed to OUT1 and OUT2 in phase because susceptances B_1 and B_2 are equal as shown in Table 1. On the other hand, if a current is imposed on IN2, out-of-phase currents are observed at the outputs because B_4 has opposite sign to B_3 causing a 180-degree phase delay. In this way, the two orthogonal excitation weights are formed by the DMN, i.e., the same principle as eigenmode decoupling [14] and

channel orthogonalization is realized by using HC [7].

We turn to the reflection characteristics. The figure clarifies the defining difference between conventional and ideal models; while the conventional model does not work properly, the ideal model offers perfect matching. This, the primary feature of the proposed technique, is due to the presence of the opposite array. The practical model also reduces reflections to under −30 dB at f_c. However, the matching effect by the proposed technique is noticeably degraded with frequency shift. Such severe frequency dependency is considered to be due to the high Q factor of the array resulting from the proximity of multi-antennas, which can be only mitigated by increasing antenna spacing or reducing number of antennas [27]. In particular, it is found that the matching bandwidth of S_{22} is narrower than that of S_{11}. As mentioned before, the Tx ports #1 and #2 correspond to even and odd modes of the connected HC. According to [28], odd-mode excitation naturally has high-Q characteristic causing a narrow bandwidth due to the relationship of $Q \propto 1/BW$ [29]. However, the practical model holds reflections lower than those without DMN over the bandwidth of 1%; the bandwidth is comparable to a channel width specified in IEEE 802.11n (20 MHz at 2.4 GHz band), one of the current WLAN standards [30].

Next, we discuss signal channel characteristics. At f_c, the ideal model exactly matches the theoretical values of the

maximum gains expressed in (12) (plotted with star marker as "Theor."). Because of the design error and losses of MSL HCs and MNs, S_{31} and S_{42} of the practical model are degraded by -0.56 dB and -0.93 dB, respectively, compared to the ideal model. Yet, they are still 1.22-dB and 2.93-dB larger than those without DMN and also surpass those achieved by the conventional DMN.

The above results verify the simultaneous decoupling and matching effects offered by the proposed techniques.

3.1.4 Channel Capacity

This subsection evaluates channel capacity characteristics. Channel capacity $C(f)$ per unit frequency at f is calculated based on Shannon's theorem as

$$C(f) = \log_2 \left| \boldsymbol{I}_{N_{\mathrm{Rx}}} + \frac{SNR}{N_{\mathrm{Tx}}} \boldsymbol{S}_{\mathrm{RT}}(f)\, \boldsymbol{S}_{\mathrm{RT}}(f)^H \right|. \quad (24)$$

where channel matrix $\boldsymbol{S}_{\mathrm{RT}}(f)$ is a function of frequency f, and $|\boldsymbol{A}|$ is a determinant of matrix $\boldsymbol{A}$. In the above equation, both Tx/Rx port numbers N_{Tx} and N_{Rx} are 2, and the signal to noise ratio, SNR, is 20 dB. Channel capacity with bandwidth BW is calculated by integrating (24) over the analysis frequency range as

$$C_{\mathrm{BW}} = \int_{BW} C(f)\, df. \quad (25)$$

Figure 10 plots channel capacity characteristics versus normalized frequency. Table 5 shows channel capacities at the center frequency, $C(f_c)$, and with bandwidth, C_{BW}. From the table, $C(f_c)$ of the ideal model completely matches the theoretical value calculated from maximum gains expressed by (12). These capacities are 21.8-% higher than that without DMN. As previous results showed, the practical model cannot match the ideal model's performance, but it yields
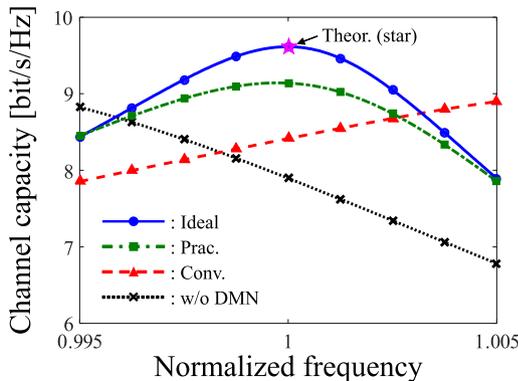
15.8-% and 8.61-% larger capacities than without DMN and with conventional DMN, respectively. From the bandwidth evaluation, the capacity of the practical model exceeds those without DMN and with conventional DMN by 11.5% and 4.41%, respectively; this superiority of the practical model over the conventional DMN model is expected to increase given the latter's lossy factors. These results prove the effectiveness of the proposed technique in terms of channel capacity improvement. Consequently, the practical implementation feasibility of the proposed technique has been demonstrated.

Although we only dealt with the simple L-shape MNs in this paper, there are much more options considering the following factors;

- the arbitrarily-settable phase in the S-parameter of the MN mentioned in Sect. 2.2
- the network topology, e.g. configuration types such as T- and π-shape, and connection types such as serial and parallel

The frequency characteristic might be improved by optimizing these factors.

3.2 Array Parameter Characteristics

This subsection evaluates performances at f_c versus some array parameters for all models. In the following analyses, conventional DMN is optimally constructed for a single array with arbitrary antenna spacing. Also, for the ideal model, optimal circuit parameters of MN are adaptively chosen depending on both antenna spacing and Tx-Rx distance. On the other hand, the practical model uses the same fixed networks as shown in Fig. 8 designed for $d = 0.25\,\lambda$ and $D = 0.1\,\lambda$; these values are defined as reference spacing and distance, respectively.

3.2.1 Impact of Antenna Spacing

First, channel capacity versus antenna spacing is plotted in Fig. 11. In the simulation, antenna spacing d is changed from $0.01\,\lambda$ to $2.0\,\lambda$ while Tx-Rx distance D is fixed at $0.1\,\lambda$.

The figure shows that the ideal model always realizes the capacity equivalent to the theoretical value, and outperforms the others over the whole analysis range. In particular, it is noteworthy that, although the capacity without DMN drops as antenna spacing becomes smaller than approximately $0.25\,\lambda$, that of the ideal model increases, a stark contrast. The other interesting characteristic is that capacities periodically fluctuate and finally converge on certain values. This can be explained by referencing the eigenmode characteristics of the channel matrix as shown in Fig. 12, where bold and dot lines indicate even and odd modes, respectively. This figure shows the following three key points.

- When antenna spacing is extremely small, strong mutual coupling and mismatching arise at Tx/Rx arrays resulting in eigenvalue degradation. Also, channel

Fig. 10 Channel capacity versus normalized frequency.
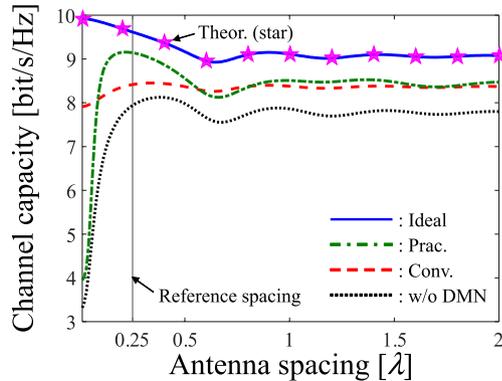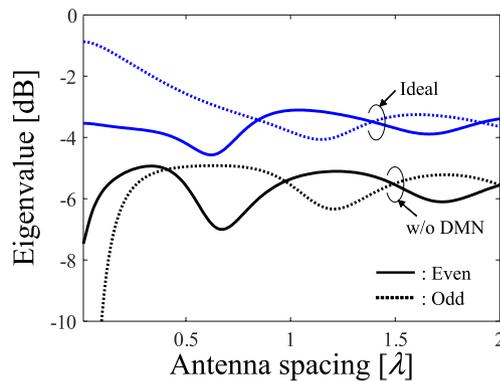
Table 5 Channel capacity.

	w/o DMN	Conv.	Prac.	Ideal	Theor.
$C(f_c)$ [bit/s/Hz]	7.90	8.42	9.14	9.62	9.62
C_{BW} [Mbit/s]	197	210	219	226	-

Fig. 11 Channel capacity versus antenna spacing.

Fig. 12 Eigenvalue versus antenna spacing.

Fig. 13 Channel capacity versus Tx-Rx distance.

components are highly correlated leading to a rank-deficient MIMO channel, all of which limit MIMO performance.

On the other hand, the eigenvalues of the ideal model (especially the odd mode) contrastingly increase as antenna spacing approaches zero; it can be regarded as the "supergain", or "superdirectivity", phenomenon that accomplishes much higher gain than that based on the classic array theory when antenna spacing is infinitesimally small and adjacent antennas have oppositely directed currents [31].

In the proposed technique, such out-of-phase current distribution is induced by odd-mode excitation using the HC. Though such a small spacing incurs high mutual coupling, the HC can actually isolate the antenna ports, and they are fully matched by the MN. In this way, the ideal model theoretically satisfies the aforementioned condition, and maximizes channel capacity by counteracting the strong mutual coupling and mismatch.

- When antenna spacing is sufficiently large, the MIMO system can be regarded as two independent SISO systems between facing Tx/Rx pairs. Hence, the two eigenvalues finally become equal and channel capacity converges to twice the capacity of one SISO link. However, cross channel components are completely diminished so infinite antenna spacing is not necessarily
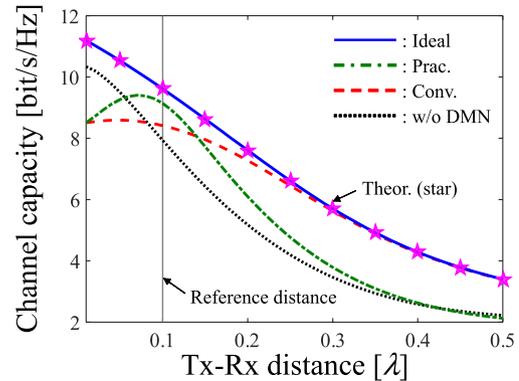
the best in term of SNR.

- In such LOS MIMO communication, a full-rank MIMO channel with two identical eigenvalues can be generated by optimizing array parameters as proven in [32]–[34]. In fact, such points can be found in the figure and capacity peaks appear near these optimal points.

Focusing on the practical model, it keeps the capacity improvement effect to some extent and outperforms the conventional DMN in the range between $0.09\,\lambda$ and $0.57\,\lambda$ even with the fixed network configuration. However, while it is comparable to the conventional DMN for wider spacing, its performance deteriorates sharply when antenna spacing is extremely small since the S-parameter of the array rapidly changes in this region.

3.2.2 Impact of Tx-Rx Distance

Channel capacity versus Tx-Rx distance is plotted in Fig. 13. In the simulation, D is varied from $0.01\,\lambda$ to $0.5\,\lambda$ while d is fixed to $0.25\,\lambda$.

As the previous result shows, the ideal model has perfect agreement with the theoretical values. In contrast, the capacity with conventional DMN drops below that without DMN when D is smaller than $0.1\,\lambda$. This is because the Tx/Rx antennas are already strongly-coupled and sufficiently-separated SISO links are established even without any decoupling countermeasure. However, when D is larger than approximately $0.25\,\lambda$, capacities of the ideal and conventional DMN models become equal. In this region, coupling between Tx/Rx arrays are negligibly, and it becomes unnecessary to consider the presence of the opposite array when designing the DMN.

From these results, the proposed technique is effective when antenna spacing and Tx-Rx distance are less than quarter-wavelength, i.e. near field communication (NFC) applications.

Finally, focusing on the practical model, its effective range where "Prac." outperforms "Conv." and "w/o DMN" is more limited between $0.06\,\lambda$ and $0.13\,\lambda$; it is an unavoidable barrier for the passive networks.

In the proposed technique, the first process using the HCs is valid regardless of the array parameters such as antenna spacing and Tx-Rx distance under the condition the whole SR-MIMO configuration is plane-symmetrical [7]. However, the problem lies in the second process using the MNs, which is influenced by the variations of the array parameters. As a promising solution for this problem, automatic matching control using variable circuit elements that responds to the array parameter variations is recommended for greater practicality [35].

4. Conclusion

This paper proposed a simultaneous decoupling and matching technique for Tx/Rx ports of SR-MIMO systems. The first process establishes parallel SISO links using hybrids and the second offers simultaneous matching in each SISO link which maximizes channel capacity. In the sense that the proposed technique fulfills both requirements, signal-and-power separation and efficiency enhancement, this idea is also applicable to simultaneous wireless information and power transfer [36].

Numerical analyses of 2×2 SR-MIMO were introduced to investigate the proposed and conventional DMN approaches in terms of (i) simultaneous decoupling and matching effects and (ii) channel capacity improvement. The results confirmed the advantage of the proposed technique given very close arrays as are common in NFC applications. Also, the successful capacity enhancement by the MSL model indicates the implementation feasibility of the proposed technique.

Experimental evaluations are required as the next step in verifying its effectiveness with more realistic RF hardware configurations in actual environments. Last but not least, the proposed technique is very sensitive to the positional error and highly frequency-dependent, so its robustness against such factors especially needs to be evaluated; these issues will be tackled in our future research.

References

[1] C. Park and T. Rappaport, "Short-range wireless communications for next-generation networks: UWB, 60 GHz millimeter-wave WPAN, and ZigBee," IEEE Wireless Commun., vol.14, no.4, pp.70–78, Aug. 2007.

[2] J.-S. Jiang and M.A. Ingram, "Spherical-wave model for short-range MIMO," IEEE Trans. Commun., vol.53, no.9, pp.1534–1541, Sept. 2005.

[3] N. Honma, K. Nishimori, T. Seki, and M. Mizoguchi, "Short range MIMO communication," Proc. 3rd EuCAP, pp.1763–1767, March 2009.

[4] K. Nishimori, N. Honma, T. Seki, and K. Hiraga, "On the transmission method for short-range MIMO communication," IEEE Trans. Veh. Technol., vol.60, no.3, pp.1247–1251, March 2011.

[5] K. Sakamoto, K. Hiraga, T. Seki, T. Nakagawa, and K. Uehara, "Performance evaluation of short-range MIMO using a method for controlling phase difference between each propagation channel," IEICE Trans. Commun., vol.E96-B, no.10, pp.2513–2520, Oct. 2013.

[6] A. Sadri, Summary of the usage models for 802.15.3c, Nov. 2006. [Online] http://www.ieee802.org/15/pub/TG3c.html

[7] K. Murata, N. Honma, K. Nishimori, and H. Morishita, "Analog eigenmode transmission for short-range MIMO," IEEE Trans. Veh. Technol., vol.65, no.1, pp.100–109, Jan. 2016.

[8] K. Murata, N. Honma, M. Tsunezawa, K. Nishimori, and H. Morishita, "Experimental evaluation of analog eigenmode transmission for short-range MIMO: Array parameter independency and wideband characteristics," IEICE ComEX, vol.4, no.6, pp.198–204, April 2015.

[9] K. Murata, N. Honma, K. Nishimori, D.M. Klymyshyn, and H. Morishita, "Four-stream parallel transmission for short-range MIMO using only passive analog components," IEICE Trans. Commun., vol.E99-B, no.1, pp.69–80, Jan. 2016.

[10] J.W. Wallace and M.A. Jensen, "Termination-dependent diversity performance of coupled antennas: Network theory analysis," IEEE Trans. Antennas Propag., vol.52, no.1, pp.98–105, Jan. 2004.

[11] J.W. Wallace and M.A. Jensen, "Mutual coupling in MIMO wireless systems: A rigorous network theory analysis," IEEE Trans. Wireless Commun., vol.3, no.4, pp.1317–1325, July 2004.

[12] B.K. Lau, J.B. Andersen, G. Kristensson, and A.F. Molisch, "Impact of matching network on bandwidth of compact antenna arrays," IEEE Trans. Antennas Propag., vol.54, no.11, pp.3225–3238, Nov. 2006.

[13] J. Weber, C. Volmer, K. Blau, R. Stephan, and M.A. Hein, "Miniaturized antenna arrays using decoupling networks with realistic elements," IEEE Trans. Microw. Theory Techn., vol.54, no.6, pp.2733–2740, June 2006.

[14] C. Volmer, J. Weber, R. Stephan, K. Blau, and M.A. Hein, "An eigen-analysis of compact antenna arrays and its application to port decoupling," IEEE Trans. Antennas Propag., vol.56, no.2, pp.360–370, Feb. 2008.

[15] J.C. Coetzee and Y. Yu, "Port decoupling for small arrays by means of an eigenmode feed network," IEEE Trans. Antennas Propag., vol.56, no.6, pp.1587–1593, June 2008.

[16] S.-C. Chen, Y.-S. Wang, and S.-J. Chung, "A decoupling technique for increasing the port isolation between two strongly coupled antennas," IEEE Trans. Antennas Propag., vol.56, no.12, pp.3650–3658, Dec. 2008.

[17] S. Roberts, "Conjugate-image impedances," Proc. IRE, vol.34, no.4, pp.198–204, April 1946.

[18] J. Rahola, "Power waves and conjugate matching," IEEE Trans. Circuits Syst. II, Exp. Briefs, vol.55, no.1, pp.92–96, Jan. 2008.

[19] N. Inagaki, "Theory of image impedance matching for inductively coupled power transfer systems," IEEE Trans. Microw. Theory Techn., vol.62, no.4, pp.901–908, Jan. 2014.

[20] K. Murata, N. Honma, K. Nishimori, and H. Morishita, "Bidirectional matching technique for Tx and Rx ports in short-range MIMO," 2014 Asia-Pacific Microwave Conference (APMC 2014), pp.498–500, Nov. 2014.

[21] TransferJet Consortium, TransferJet whitepaper, Sept. 2015. [Online] https://www.transferjet.org/tj/transferjet_whitepaper.pdf

[22] G.R. Simpson, "A generalized n-port cascade connection," MTT-S International Microwave Symposium Digest, pp.507–509, 1981.

[23] D.M. Pozar, Microwave Engineering, 4th ed., Wiley, New York, 2012.

[24] C.-H. Liang, Y. Shi, and T. Su, "S parameter theory of lossless block network," Progress In Electromagnetics Research, vol.104, pp.253–266, 2010.

[25] G.J. Burke and A.J. Poggio, "Numerical electromagnetics code (NEC)-method of moments," Lawrence Livermore Lab., Livermore, CA, Rep. UCID18834, Jan. 1981.

[26] Mentor Graphics, The IE3D$^{\text{TM}}$ electromagnetic design. [Online] http://www.mentor.com/electromagnetic-simulation/

[27] J.C. Coetzee and Y. Yu, "Design of decoupling networks for circulant symmetric antenna arrays," Antennas Wirel. Propag. Lett., vol.8, pp.291–294, May 2009.

[28] K. Wang, L. Li, and T.F. Eibert, "Comparison of compact monopole antenna arrays with eigenmode excitation and multiport conjugate

matching," IEEE Trans. Antennas Propag., vol.61, no.8, pp.4054–4062, Aug. 2013.

[29] A.D. Yaghjian and S.R. Best, "Impedance, bandwidth, and Q of antennas," IEEE Trans. Antennas Propag., vol.53, no.4, pp.1298–1324, April 2005.

[30] [Online] http://www.ieee802.org/11/

[31] C.A. Balanis, Antenna Theory: Analysis and Design, 3rd ed., Wiley, New York, 2005.

[32] L. Liu, W. Hong, H. Wang, G. Yang, N. Zhang, H. Zhao, J. Chang, C. Yu, X. Yu, H. Tang, H. Zhu, and L. Tian, "Characterization of line-of-sight MIMO channel for fixed wireless communications," Antennas Wirel. Propag. Lett., vol.6, no.11, pp.36–39, March 2007.

[33] F. Bøhagen, P. Orten, and G.E. Øien, "Design of optimal high-rank line-of-sight MIMO channels," IEEE Trans. Wireless Commun., vol.6, no.4, pp.1420–1425, April 2007.

[34] I. Sarris and A.R. Nix, "Design and performance assessment of high-capacity MIMO architectures in the presence of a line-of-sight component," IEEE Trans. Veh. Technol., vol.56, no.4, pp.2194–2202, July 2007.

[35] X. Tang, K. Mouthaan, and J.C. Coetzee, "Tunable decoupling and matching network for diversity enhancement of closely spaced antennas," Antennas Wirel. Propag. Lett., vol.11, pp.268–271, Feb. 2012.

[36] S. Timotheou, I. Krikidis, S. Karachontzitis, and K. Berberidis, "Spatial domain simultaneous information and power transfer for MIMO channels," IEEE Trans. Wireless Commun., vol.14, no.8, pp.4115–4128, March 2015.

Appendix A: Derivation of (6)

This appendix derives the S-parameter expression of cascade-connected networks given as (6). We assume that three arbitrary networks A, B and C, and their S-parameters are expressed as

$$S_X = \begin{bmatrix} S_{X,ii} & S_{X,io} \\ S_{X,oi} & S_{X,oo} \end{bmatrix} \tag{A·1}$$

where index "X" is replaced A, B or C indicating network sign.

When networks A and B are cascade-connected as shown in Fig. A·1(a), the complete S-parameter is given as (A·2) at the bottom of this page. Equation (A·2) is a modified version of the expression shown in [22] (the original expression is somewhat complicated due to confusing port definition.) Also, same expressions can be seen in [10] and [11].

Specifically, in the case that network A has neither reflection nor coupling at its inputs and outputs, i.e. $S_{A,ii}$ and $S_{A,oo}$ are zero matrices, (A·2) can be expressed more simply as

$$S = \begin{bmatrix} S_{A,io}S_{B,ii}S_{A,oi} & S_{A,io}S_{B,io} \\ S_{B,oi}S_{A,oi} & S_{B,oo} \end{bmatrix} . \tag{A·3}$$

From the above equation, the rules of the cascade-connection in this situation are summarized as follows.

(a) two cascade-connected networks.

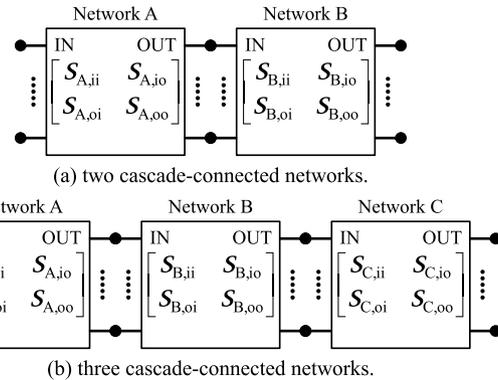(b) three cascade-connected networks.

Fig. A·1 Cascade-connected multiple networks.

With regard to the S-parameter of the cascade-connected networks,

- the reflection-and-coupling submatrix at the ports with the matched-and-decoupled network connected is sandwiched by its transmission matrices from both left and right sides.
- the reflection-and-coupling submatrix at the other ports remains unaltered.
- the transmission submatrices between inputs and outputs of the whole system are expressed by multiplexing the transmission matrices of the two networks. The order of matrix multiplication depends on from which side the matched-and-decoupled network is connected.

Based on the above rules, when three networks A, B, and C are cascade-connected as shown in Fig. A·1(b), and networks A and C have neither reflection nor mutual coupling, the complete S-parameter of the whole system is given as

$$S = \begin{bmatrix} S_{A,io}S_{B,ii}S_{A,oi} & S_{A,io}S_{B,io}S_{C,io} \\ S_{Coi}S_{B,oi}S_{A,oi} & S_{C,oi}S_{B,oo}S_{C,io} \end{bmatrix} . \tag{A·4}$$

Again, the ports of the ideal hybrid are perfectly matched and decoupled. Thus, (6) is justified in the proposed technique.

Appendix B: Channel Capacity with Ideal HCs

The channel matrix when the HCs are connected to Tx/Rx sides, S'_{RT}, is expressed as

$$S'_{RT} = S_{HC,oi}S_{RT}S_{HC,oi} \tag{A·5}$$

as derived in Appendix A.

Based on Shannon's theorem, the channel capacity of the 2×2 MIMO system after the HCs are connected is calculated as

$$S = \begin{bmatrix} S_{A,ii} + S_{A,io}\left(I - S_{B,ii}S_{A,oo}\right)^{-1}S_{B,ii}S_{A,oi} & S_{A,io}\left(I - S_{B,io}S_{A,oo}\right)^{-1}S_{B,io} \\ S_{B,oi}\left(I - S_{A,oo}S_{B,ii}\right)^{-1}S_{A,oi} & S_{B,oo} + S_{B,oi}\left(I - S_{A,oo}S_{B,ii}\right)^{-1}S_{A,oo}S_{B,io} \end{bmatrix} . \tag{A·2}$$

$$C = \log_2 \left| \boldsymbol{I}_2 + \frac{SNR}{2} \boldsymbol{S}'_{\text{RT}} \boldsymbol{S}'^{H}_{\text{RT}} \right| \qquad (\text{A}\cdot 6)$$

$$= \log_2 \left| \boldsymbol{I}_2 + \frac{SNR}{2} \boldsymbol{S}_{\text{HC,oi}} \boldsymbol{S}_{\text{RT}} \boldsymbol{S}_{\text{HC,oi}} \boldsymbol{S}^{H}_{\text{HC,oi}} \boldsymbol{S}^{H}_{\text{RT}} \boldsymbol{S}^{H}_{\text{HC,oi}} \right|.$$

Remember that $\boldsymbol{S}_{\text{HC,oi}}$ is unitary, i.e. $\boldsymbol{S}_{\text{HC,oi}} \boldsymbol{S}^{H}_{\text{HC,oi}} = \boldsymbol{I}_2$. Thus, the above equation is rewritten as

$$C = \log_2 \left| \boldsymbol{S}_{\text{HC,oi}} \boldsymbol{S}^{H}_{\text{HC,oi}} + \frac{SNR}{2} \boldsymbol{S}_{\text{HC,oi}} \boldsymbol{S}_{\text{RT}} \boldsymbol{S}^{H}_{\text{RT}} \boldsymbol{S}^{H}_{\text{HC,oi}} \right| \quad (\text{A}\cdot 7)$$

$$= \log_2 \left| \boldsymbol{S}_{\text{HC,oi}} \left(\boldsymbol{I}_2 + \frac{SNR}{2} \boldsymbol{S}_{\text{RT}} \boldsymbol{S}^{H}_{\text{RT}} \right) \boldsymbol{S}^{H}_{\text{HC,oi}} \right|.$$

Further, by the use of following two fundamental theorems of determinants;

- the determinant of the product is equal to the product of the determinants, i.e. $|\boldsymbol{AB}| = |\boldsymbol{A}||\boldsymbol{B}|$
- the product of the determinants is commutative, i.e. $|\boldsymbol{A}||\boldsymbol{B}| = |\boldsymbol{B}||\boldsymbol{A}|$

where $\boldsymbol{A}$ and $\boldsymbol{B}$ are square matrices of the same order, (A·7) is factorized as

$$C = \log_2 \left| \boldsymbol{S}_{\text{HC,oi}} \right| \left| \boldsymbol{I}_2 + \frac{SNR}{2} \boldsymbol{S}_{\text{RT}} \boldsymbol{S}^{H}_{\text{RT}} \right| \left| \boldsymbol{S}^{H}_{\text{HC,oi}} \right| \qquad (\text{A}\cdot 8)$$

$$= \log_2 \left| \boldsymbol{S}_{\text{HC,oi}} \boldsymbol{S}^{H}_{\text{HC,oi}} \right| \left| \boldsymbol{I}_2 + \frac{SNR}{2} \boldsymbol{S}_{\text{RT}} \boldsymbol{S}^{H}_{\text{RT}} \right|.$$

Again, $\boldsymbol{S}_{\text{HC,oi}} \boldsymbol{S}^{H}_{\text{HC,oi}} = \boldsymbol{I}_2$, so the first determinant term in the above equation becomes one. Finally, we obtain

$$C = \log_2 \left| \boldsymbol{I}_2 + \frac{SNR}{2} \boldsymbol{S}_{\text{RT}} \boldsymbol{S}^{H}_{\text{RT}} \right|, \qquad (\text{A}\cdot 9)$$

which is exactly the same as the channel capacity of the 2×2 MIMO system before the HCs are connected. Hence, channel capacity is constant before and after the HCs are connected.

Kentaro Murata received the B.E. and M.E. degrees in electrical and electronics engineering from Iwate University, Morioka, Japan in 2011 and 2014, respectively. He is currently working toward the Ph.D. degree with Graduate School of Science and Engineering, National Defense Academy of Japan, Yokosuka, Japan. His current research interests include feeding methods for multiple-input-multiple-output antenna systems.

Naoki Honma received the B.E., M.E., and Ph.D. degrees in electrical engineering from Tohoku University, Sendai, Japan in 1996, 1998, and 2005, respectively. In 1998, he joined the NTT Radio Communication Systems Laboratories, Nippon Telegraph and Telephone Corporation (NTT), in Japan. He is now working for Iwate University. He received the Young Engineers Award from the IEICE of Japan in 2003, the APMC Best Paper Award in 2003, the Best Paper Award of IEICE Communication Society in 2006, and the APMC Best Paper Award in 2014, respectively. His current research interest is MIMO antennas for high-speed wireless communication systems.

Kentaro Nishimori received the B.E., M.E. and Ph.D. degrees in electrical and computer engineering form Nagoya Institute of Technology, Nagoya, Japan in 1994, 1996 and 2003, respectively. In 1996, he joined the NTT Wireless Systems Laboratories, Nippon Telegraph and Telephone Corporation (NTT), in Japan. He was senior research engineer on NTT Network Innovation Laboratories. He is now associate professor in Niigata University. He was a visiting researcher at the Center for Teleinfrastructure (CTIF), Aalborg University, Aalborg, Denmark from Feb. 2006 to Jan. 2007. He was an Associate Editor for the Transactions on Communications for the IEICE Communications Society from May 2007 to May 2010 and Assistant Secretary of Technical Committee on Antennas and Propagation of IEICE from June 2008 to May 2010. He received the Young Engineers Award from the IEICE of Japan in 2001, Young Engineer Award from IEEE AP-S Japan Chapter in 2001, Best Paper Award of Software Radio Society in 2007 and Distinguished Service Award from the IEICE Communications Society in 2005, 2008 and 2010. His main interests are spatial signal processing including MIMO systems and interference management techniques in heterogeneous networks. He is a member of IEEE and IEICE. He received IEICE Best Paper Award in 2010.

Naobumi Michishita received the B.E., M.E. and D.E. degrees in electrical and computer engineering from Yokohama National University, Yokohama, Japan, in 1999, 2001, and 2004, respectively. In 2004, he was a research associate at the Department of Electrical and Electronic Engineering, National Defense Academy, Kanagawa, Japan, where he is currently an associate professor. From 2006 to 2007, he was a visiting scholar at the University of California, Los Angeles. His current research interests include metamaterial antenna and electromagnetic analysis. He is a member of the Institute of Electronics, Information and Communication Engineers (IEICE), Japan. He is also members of the Japan Society for Simulation Technology and the Institute of Electrical and Electronics Engineers (IEEE). He was the recipient of the Young Engineer Award presented by the IEEE Antennas and Propagation Society Japan Chapter and the IEICE, Japan (2004 and 2005). He received the best paper award and the best tutorial paper award from the IEICE Communication Society in 2013 and 2014, respectively.

Hisashi Morishita received the B.S. degree in Electrical Engineering from National Defense Academy of Japan in 1980, the M.S. and Ph.D. degrees from University of Tsukuba in 1987 and 1990, respectively. From 1990 to 1992, he worked as a research and development officer at Air Research and Development Command of Japan Air Self-Defense Force (JASDF). Since 1992, he has been with National Defense Academy and is currently a Professor in the Department of Electrical and Electronic Engineering. From 1996 to 1997, he was a Visiting Researcher at the Communications Research Laboratory, McMaster University, Canada. His research is concerned with mobile communication and small antennas. He is a fellow of IEICE and a senior member of IEEE.